

2001-GT-0307

**UNSTEADY AERODYNAMICAL BLADE ROW INTERACTION
IN A NEW MULTISTAGE RESEARCH TURBINE
PART 2: NUMERICAL INVESTIGATION**

Wolfgang Höhn

MTU Aero Engines

Department of Aeroelasticity and Acoustics
Dachauer Straße 665, D-80995 München
Germany

Email: wolfgang.hoehn@muc.mtu.de

Ralf Gombert and Astrid Kraus

Institute of Aeronautical Propulsion
University of Stuttgart
Pfaffenwaldring 6, D-70569 Stuttgart
Germany

ABSTRACT

This paper is the second part of a two part paper, which describes in part one the experimental setup and results of a new multistage turbine. Part two presents results of unsteady viscous flow calculations based on cold flow experiments of that three stage low pressure turbine. The present paper emphasizes the investigation of stator-stator interaction of a low pressure turbine section of a commercial jet engine. Different positions for the second and third stator are studied numerically and experimentally with respect to the blade row interaction, unsteady blade loading and unsteady boundary layer effects.

A time accurate Reynolds averaged Navier-Stokes solver is applied for the computations. Turbulence is modeled using the Spalart-Allmaras one equation model turbulence model and the influence of modern transition models on the unsteady flow predictions is investigated. The integration of the governing equations in time is performed by a four stage Runge-Kutta scheme, which is accelerated by a two grid method in the viscous boundary layer around the blades and alternatively by a dual time stepping method. At the inlet and outlet reflecting or non-reflecting boundary conditions are used. The quasi 3D calculations are conducted on a stream surface around midspan allowing a varying stream tube thickness.

In particular, the flow field with respect to time averaged and unsteady quantities such as surface pressure, vorticity, unsteady velocity field and skin friction are compared with the experiments conducted in the cold air flow test rig.

NOMENCLATURE

C_{abs} velocity
MMG meridional coordinate
P pressure
 $q_{\tau_w} = ((E^2 - E_0^2)/E_0^2)^3$ quasi wall shear stress
t time
T blade passing period
 U_m phase averaged hot film output voltage
 U_{rms} random hot film output voltage
 μ_T dynamic viscosity
 τ_w wall shear stress
Subscript
e entrance flow quantity
s static flow quantity
t stagnation flow quantity
v vane

INTRODUCTION

Many research activities are presently conducted in the field of unsteady blade row interaction in axial turbomachines, e.g. Halstead et al. (1997), Hodson (1998), Fan and Lakshminarayana (1996), Sharma (1998) and Solomon (2000).

The aim of this paper is to present the results of a computational method (Eulitz and Engel, 1998) which quantitatively predicts important unsteady transition effects in a three stage low pressure turbine. The Abu-Ghannam and Shaw (1980) model is

used to predict the onset of transition. It is one of the widely-used models in both external and internal flow simulations (Coupland, 1995). A modification of the Abu-Ghannam Shaw model conducted by Drela (1995) has been implemented into the used Navier-Stokes solver (Eulitz et al., 1998). Other approaches found in the literature either use algebraic turbulence models in conjunction with the intermittency approach (Narasimha, 1990) or two equation models, especially the low Reynolds number $k-\epsilon$ models (Savil, 1994). Eulitz and Engel (1998) and Eka-terinaris (1995) demonstrated for turbomachinery and airfoil applications that the one-equation turbulence model of Spalart and Allmaras (1992) is a good compromise between turbulent prediction qualities and computational costs.

The present work is conducted within the German Engine-3E turbine technology program (Niehuis, 1997). The final goal of this project is to understand the underlying mechanisms of turbine stator clocking, which denotes the interaction of an upstream wake of a stator with the next stator, which has the same blade count. Although several studies on turbine clocking have been presented (Dorney and Sondak, 2000; Dorney et al., 1999; Huber et al., 1995), the phenomenon is not fully understood yet.

After the description of the experimental setup, the computational method used for steady and unsteady computations is explained. The latter needs a steady state initial solution for the time-accurate computation of the unsteady Reynolds averaged Navier-Stokes equations. Moreover, the turbulence and transition model which are used are discussed. Finally, the results of the steady state, time averaged unsteady and unsteady calculations are compared with experiments conducted in a low pressure turbine cold flow turbine test rig.

EXPERIMENTAL SETUP

The investigations are performed in a 3-stage cold-air LPT rig with various operating conditions, see also part one of this paper. All three stators carry the same number of vanes which can be precisely adjusted circumferentially, see figure 1. In addition to the Reynolds number the wheel speed can be varied.

Instrumentation and Measurements

The test rig is instrumented in order to study the physics of stator clocking. The total isentropic efficiency is determined by measuring the representative total pressure and total temperature at the turbine inlet and outlet, where mixing losses are not taken into account. Since the inflow conditions to the downstream stator of each clocking pair vary for the circumferential positions comprehensive unsteady instrumentation is provided at mid span. The leading edges are fitted with steady total pressure probes, the suction sides as well as the pressure sides of the profiles are equipped with surface mounted hot-film sensors. Static pressure holes are used to measure the time averaged pressure on

the stator blades at midspan. Behind each stator and the last rotor the total pressure and total temperature as well as all velocity components of the flow are measured. Hot film probes are used to detect the position of the wake of upstream stator blades at downstream stator blades.

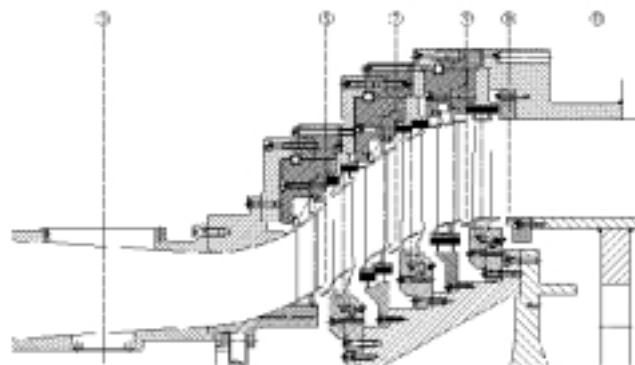


Figure 1. *EXPERIMENTAL SETUP.*

COMPUTATIONAL METHOD

The unsteady flow equations, i.e. the Reynolds-averaged, compressible Navier-Stokes equations, are solved along the three-dimensional stream-tube with varying radial thickness and radius (Eulitz and Engel, 1998). The convective fluxes are discretized using Roe's upwind scheme (Roe, 1991) in combination with van Leer's MUSCL approach (van Leer, 1979) to obtain second order accuracy in space. The viscous terms are discretized with central differences. At the solid blade wall the no-slip condition is used. At the streamtube boundaries towards the tip and the hub the kinematic boundary condition is applied. The steady state equations are marched in time using an implicit scheme (Eulitz et al., 1998). The unsteady flow equations are solved using a four stage Runge-Kutta scheme in combination with He's time accurate two-grid method (He, 1993). For the steady state solution at the inlet and outlet boundaries of the computational domain, quasi-three dimensional non-reflecting boundary conditions are applied (Saxer and Giles, 1993). For the unsteady computations non-reflecting boundary conditions according to Hoying (1997) as well as reflecting boundary conditions based on Riemann invariants can be used. At the rotor-stator interface the sheared cell technique (Giles, 1991) is employed for the unsteady computations, whereas the circumferential averaged characteristic variables are exchanged at the steady rotor-stator interface.

The used multi-block solver is parallelized based on domain decomposition and message passing using communication routines of the MPI library. In order to achieve good parallel performance and efficiency, explicit or block local solution strategies are implemented (Engel et al., 1996).

Turbulence and Transition Modeling

In order to close the Reynolds averaged Navier-Stokes equations the Boussinesq hypothesis is used (Bousinesq, 1877) together with the Spalart and Allmaras one equation turbulence model (Spalart and Almaras, 1992).

Transition onset is determined from a correlation as proposed by Drela (1995) for his viscous/inviscid interaction code MISES, which is a modification of the well known Abu-Ghanam Shaw (1980) criterion. In the laminar part of the boundary layer the transport equation of the one equation turbulence model is solved without turbulent production. When the Drela correlation signals the start of transition, the production term is switched on.

Configuration and Computational Mesh

A low pressure model turbine with 3 stages, as shown in figure 2, is considered for this study. A blade count ratio of 1 has been assumed in order to limit the computational costs. The 96 rotor blades were geometrically scaled to a blade number of 102, i.e. the number of stator blades, in order to keep loading of the blades the same as in the unscaled case. Moreover, the axial gaps between the blades in the calculations are kept the same as in the experiments. The Mach number at the entry of the turbine is 0.2 and the total pressure ratio is approximately 1.3. The Reynolds number based on the exit flow and the chord length of the first vane is 180000. For the turbulent calculation using the transition model the turbulence level is 2.5 % at the inlet of the computational mesh. The computational mesh consists of two O-blocks around the airfoils and four H-blocks in the blade passage with a total number of 21000 mesh cells for each blade passage. The y^+ values of the first mesh points off the surface are below 1.25 in order to accurately resolve the turbulent boundary layer and 20 to 35 mesh points are in the boundary layer in the aft section of the blades.

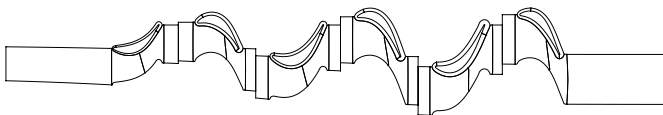


Figure 2. *COMPUTATIONAL MESH.*

Figures 3 and 4 show the details of the mesh for stator 2. Around the blade 250 points on the profile are used. In order to resolve the vorticity- and pressure waves accurately 70 mesh points are used in the H-mesh in the pitchwise direction.

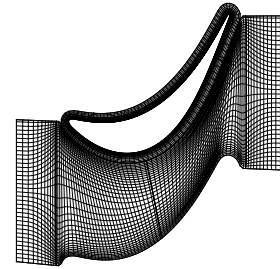


Figure 3. *COMPUTATIONAL MESH STATOR 2, every 2nd mesh point shown.*

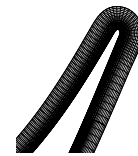


Figure 4. *COMPUTATIONAL MESH STATOR 2, trailing edge.*

Steady State Calculation

The steady state multistage calculation is initialized by linear interpolation of the calculated flow angle and Mach number and pressure for each blade by the values obtained from the S2 design procedure used at MTU. The Reynolds averaged Navier-Stokes equations are marched in time by a fully implicit time integration scheme (Eulitz et al., 1998). For the fully turbulent calculations approx. 3000 timesteps are needed to achieve full convergence using a CFL number of 10. For the calculations using the transition correlation the first 500 time steps are used to develop the turbulent boundary layer and then approx. 5000 time steps are required to achieve a converged steady state solution. At the stator-rotor interface passage averaged flow quantities are exchanged and the wakes are mixed out at the blade row boundaries. The steady state calculation is used as initial solution for the unsteady time accurate calculations.

Time-Accurate Calculation

When starting the unsteady calculation with the steady state result as initial solution, a time periodic solution does not evolve until all wakes are convected through the computational domain. Using the two-grid method the timestep can be set to a CFL number of 6.0 in the O-grid, where the smallest cells are found in the viscous boundary layer. 24 blade passing periods are computed to obtain a periodic unsteady flow field, which is proved by the computation of the unsteady overall efficiency. The unsteady calculations are mainly performed on a CRAY T3E using up to 44

processors.

RESULTS

Steady State Results

In order to study the basic performance of the transition model steady state calculations are performed for the complete setup on the streamline around midspan in a Q3D fashion. The boundary conditions for the numerical computations are taken from the S2 design method used at MTU.

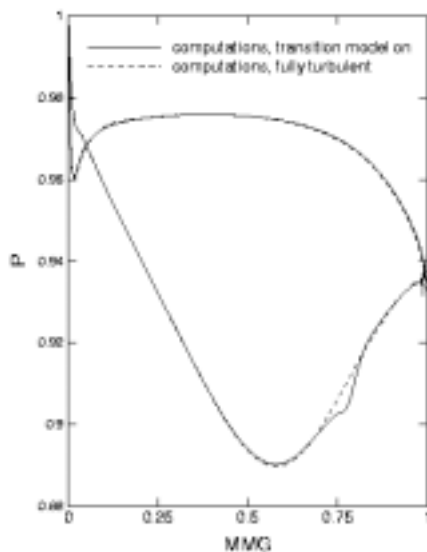


Figure 5. *STEADY STATE SURFACE PRESSURE DISTRIBUTION, STATOR 1.*

Figure 5, 6 and 7 show the surface pressure distribution at midspan for the stator blades normalized with the total inlet pressure. Good agreement between the time averaged unsteady measurements and the steady calculation is found in general.

The steady computations show no significant differences between the fully turbulent computations and the results obtained using the transition model. Only, in the rearward region of the suction side differences are found in the pressure distribution indicating the transition from laminar to turbulent flow: Close to the trailing edge on the suction side of the first stator blade the laminar flow separates, transition occurs and the turbulent flow reattaches again. On the suction side of stator 2 and stator 3 only a very small transition like pressure distribution is found at $MMG = 0.75$. The flow does not separate, which is confirmed by the experimental investigations.

Time Averaged Unsteady Results

The figure 8, 9 and 10 show the time averaged surface pressure distribution for the experiments and the computations con-

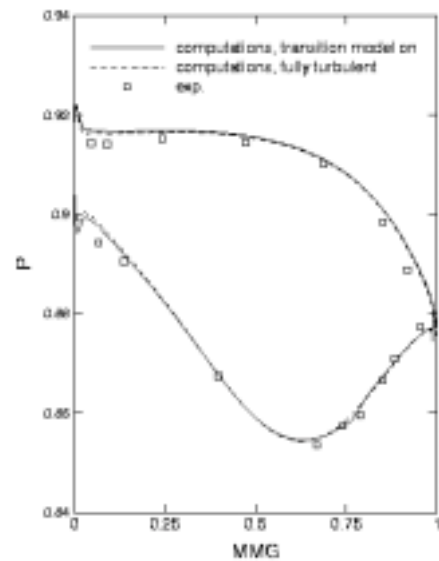


Figure 6. *STEADY STATE SURFACE PRESSURE DISTRIBUTION, STATOR 2.*

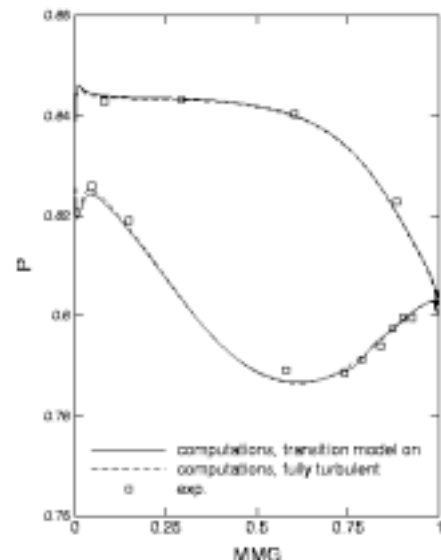


Figure 7. *STEADY STATE SURFACE PRESSURE DISTRIBUTION, STATOR 3.*

ducted using the Navier-Stokes equations incorporating the transition model for the stators of the low pressure rig at midspan. In general good agreement with the experiments is found for a certain stator position (stator one in position a, i.e. the same as in part one of this paper), which confirms the applicability of the used quasi three-dimensional method towards the investigated problem. The time averaged unsteady results are close to the steady results, which indicates no large non-linear unsteady effects.

Only stator two and three show small differences between the steady and the time averaged unsteady results due to the un-

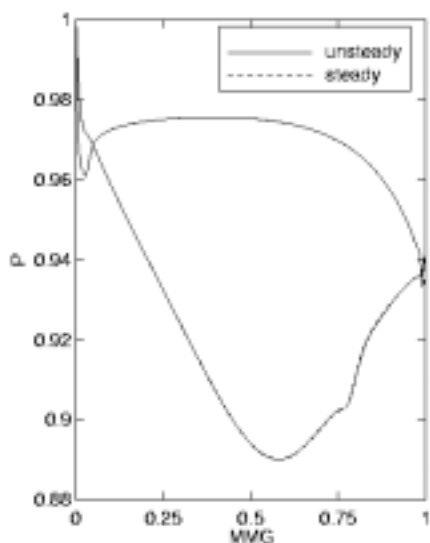


Figure 8. *TIME AVERAGED SURFACE PRESSURE DISTRIBUTION, STATOR 1.*

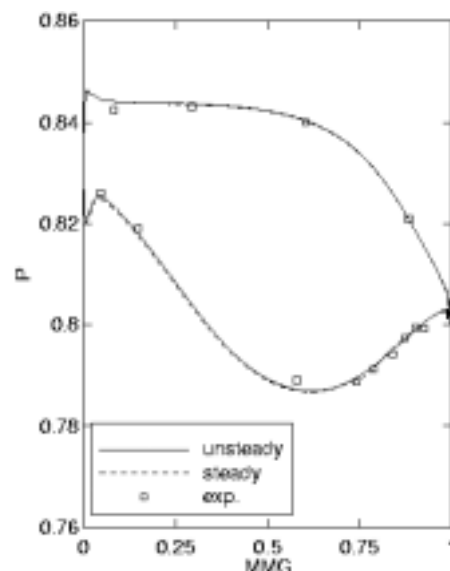


Figure 10. *TIME AVERAGED SURFACE PRESSURE DISTRIBUTION, STATOR 3.*

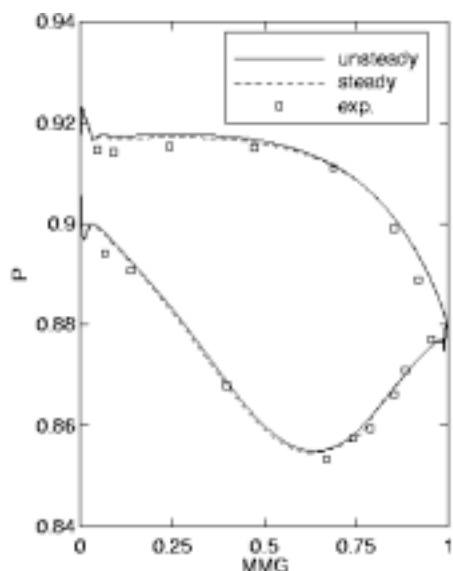


Figure 9. *TIME AVERAGED SURFACE PRESSURE DISTRIBUTION, STATOR 2.*

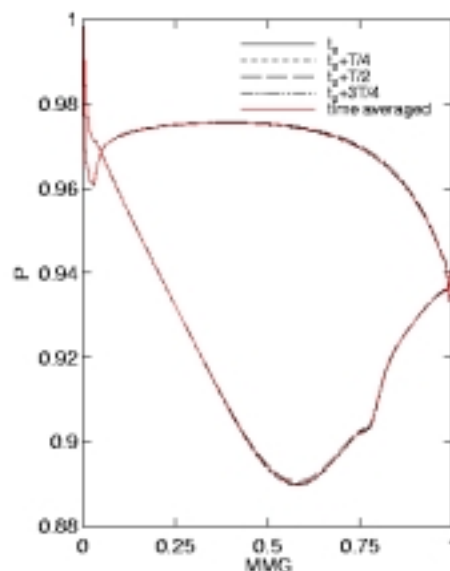


Figure 11. *UNSTEADY SURFACE PRESSURE DISTRIBUTION, STATOR 1.*

steady interaction of the rotor wakes with the downstream stator (see also figures 11, 12 and 13).

Unsteady Results

The figures 11, 12 and 13 show the unsteady surface pressure distribution for the computations conducted using the Navier-Stokes equations incorporating the transition model for the stators of the low pressure rig at midspan at four time steps during one blade passing period T in comparison with the time averaged unsteady results.

The results on stator one show no major difference between the unsteady and the time averaged results. This is due to the fact that the stator feels only minor influence on the rear suction side due to upstream running pressure waves of the first rotor. The wakes of the upstream rotor of stator 2 and 3 create a stronger unsteady surface pressure distribution, which is due to the time varying incoming flow for the stator 2 and 3 and yields a moving of the pressure minimum on the suction side of the stator blades in time. However, the time mean of the surface distribution differs only slightly from the steady pressure distribution.

Corresponding results give a Fourier decomposition in time

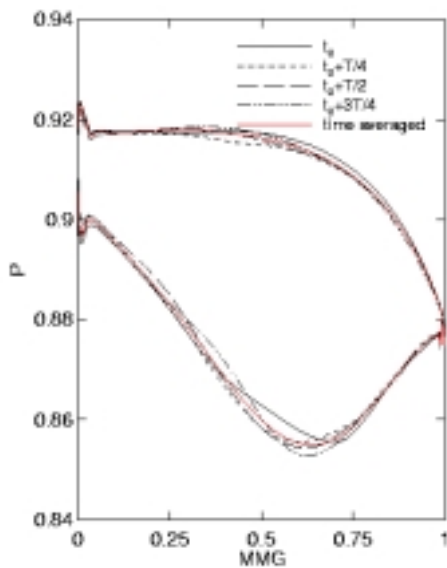


Figure 12. UNSTEADY SURFACE PRESSURE DISTRIBUTION, STATOR 2.

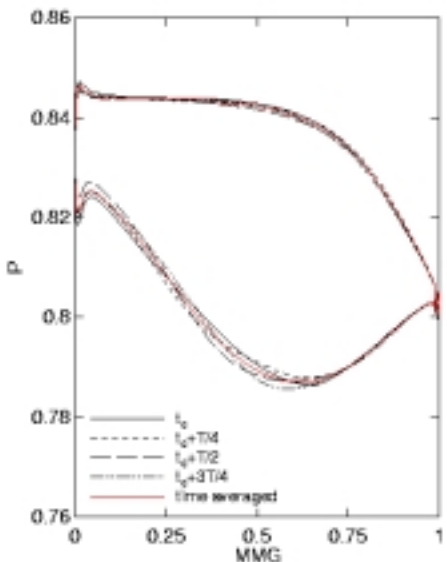


Figure 13. UNSTEADY SURFACE PRESSURE DISTRIBUTION, STATOR 3.

for the unsteady static surface pressure distribution of stator 2 in figure 14, where only the pressure amplitudes are shown. The fundamental component has higher amplitudes for a meridional coordinate $MMG = 0.2$ up to $MMG = 0.8$ on the suction side with a maximum at $MMG=0.5$, which is consistent to the high unsteady pressure fluctuations at these axial positions. The maximum is approximately at the same position on the pressure side with an amplitude of about 1/3 of the peak value on the suction side. Another maximum is found at the leading edge due to the passing of the rotor wake with about the same amplitude as the respective values on the suction and the pressure side around

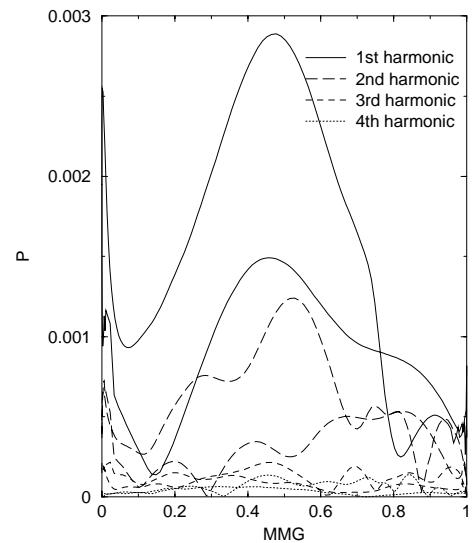


Figure 14. UNSTEADY SURFACE PRESSURE Fourier decomposition, STATOR 2.

midchord. The 2nd harmonic has about 1/3 of the amplitude of the 1st harmonic on the suction as well as on the pressure side. The higher harmonics are much smaller and can be neglected.

Figures 15, 16, 17 and 18 show the different vortex structure of the wakes represented as vorticity leaving the blades and impinging on the downstream blade row at different time instants during one blade passing period T . Of interest is, for example, the wake of the first stator (S1). It consists of a double vortex, which is seen as a red and blue part of the wake leaving the stator one blade row representing counter-rotating vortices. The stator 1 wake is interacting then with rotor one and its boundary layer. As seen from the different time instants the stator wake is stretched and distorted by the so called negative jet effect in the rotor passage. For the given stator one position (stator one in position a) the wake enters the passage of stator 2 (S1 in figure 15) and passes along the rearward section of the suction side of stator 2 (S1 in figure 16). This is also evident in figure 23, where the stator 1 wake (S1) leads to higher wall shear stresses. As the wake of stator 1 moves further it shows some tendency to merge with the wake of rotor 1 (R1+S1 in figure 18). A very similar interaction process takes place within the next three blade rows, i.e. stator 2, rotor 2 and stator 3. However, due to the interaction of the wakes with the upstream wakes it is more difficult to clearly identify the origin of each wake.

In front of the stator 2 leading edge, see the cross in the figures 21 and 22, a hot film probe is mounted in order to detect the wake of stator 1 and rotor 1.

Figure 19 and figure 20 show the computed absolute velocity C_{abs} and the computed viscosity μ_T together with the phase averaged anemometer output voltage U_m and the random unsteadiness of the anemometer output voltage U_{rms} in the s1-plane at midspan for three blade passing periods. Good agreement in

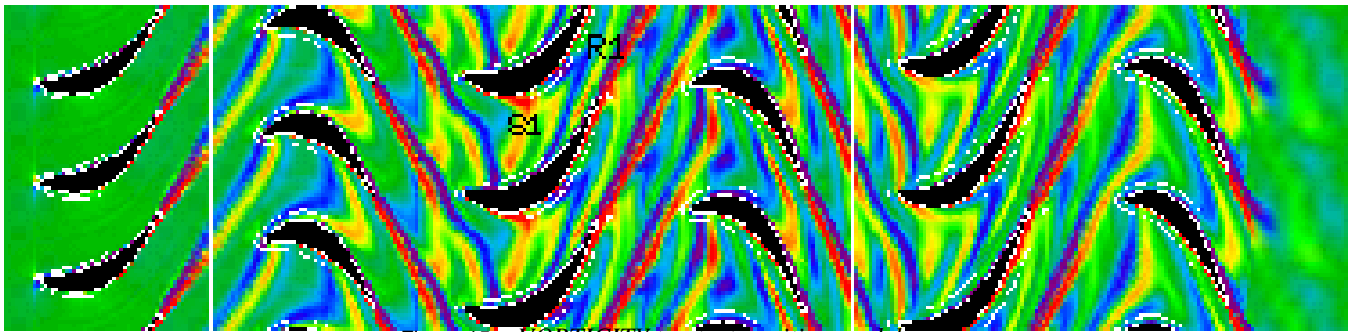


Figure 15. *VORTICITY* $t = t_0$, transition model on.

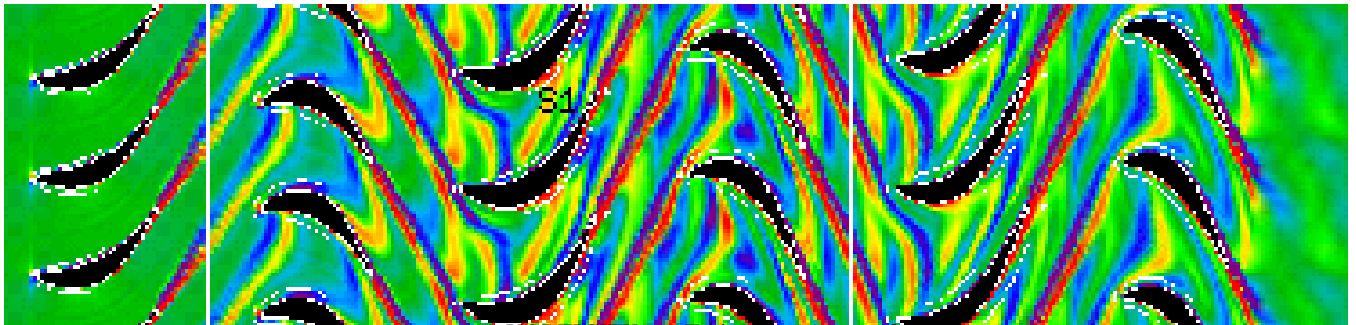


Figure 16. *VORTICITY* $t = T/4$, transition model on.

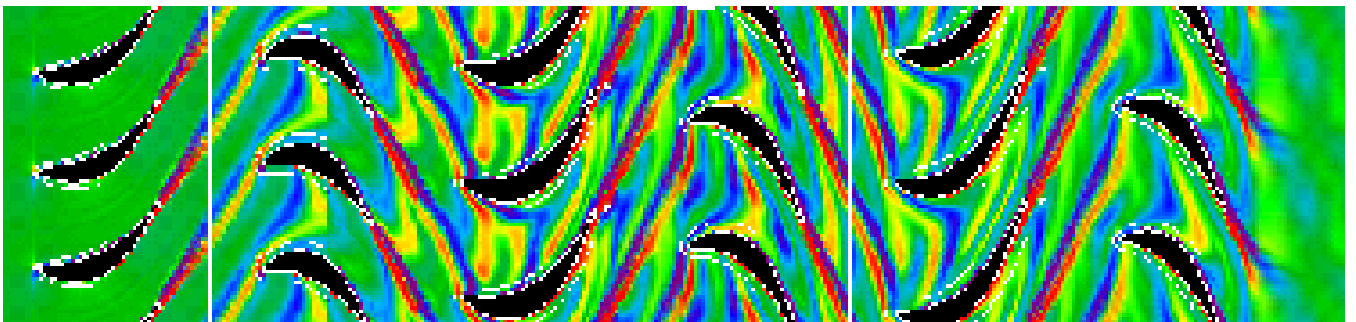


Figure 17. *VORTICITY* $t = T/2$, transition model on.

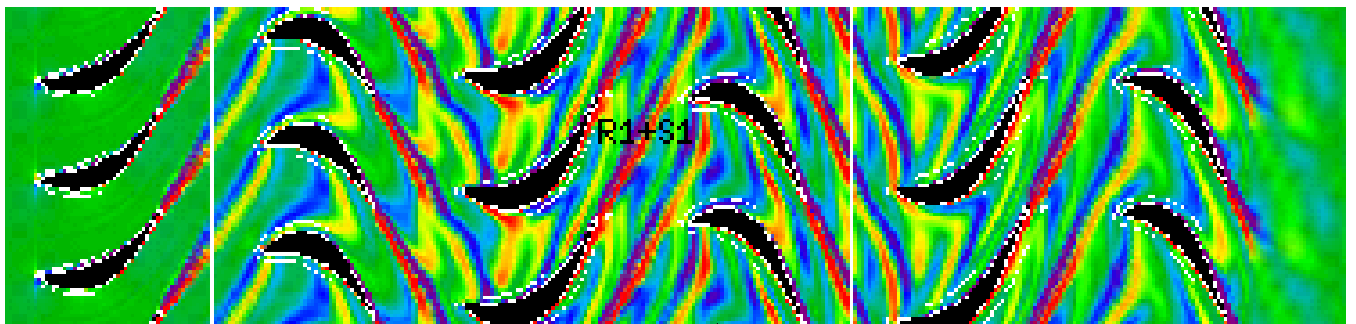


Figure 18. *VORTICITY* $t = 3T/4$, transition model on.

phase is found between the computed rotor wake (R1) represented as minimum in the velocity plot, the computed maximum of the viscosity, the maximum of the phase averaged anemometer output voltage and the random unsteadiness of the anemometer output voltage due to the rotor wake (R1). The results are consistent with the contour plots given in figure 21 and figure 22, where

the vorticity is shown for $t/T=0.28$ and $t/T=0.73$. At $t/T=0.73$ the rotor wake (blue vortex) hits the hot film probe and yields high anemometer output voltage. Figure 19 and figure 20 show also the wake of stator 1 (S1), which can also be seen in figure 21 right in front of the hot film probe (cross). The stator 1 wake (S1) creates a local minimum in the computed velocity, see S1

in figure 19, and a local maximum in figure 20 for the phase averaged anemometer output voltage U_m and random unsteadiness U_{rms} . However, the computed viscosity in figure 20 shows only one maximum, rather than two due to the rotor 1 and stator 1 wake.

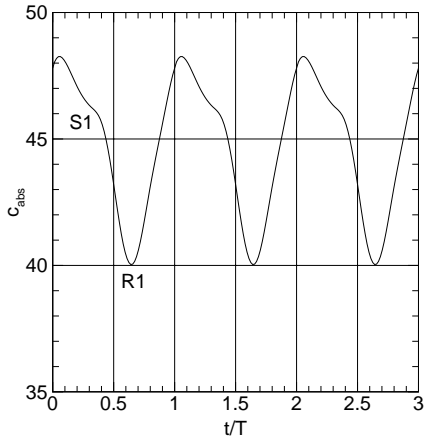


Figure 19. HOT FILM PROBE, inlet stator 2, computed velocity C_{abs} .

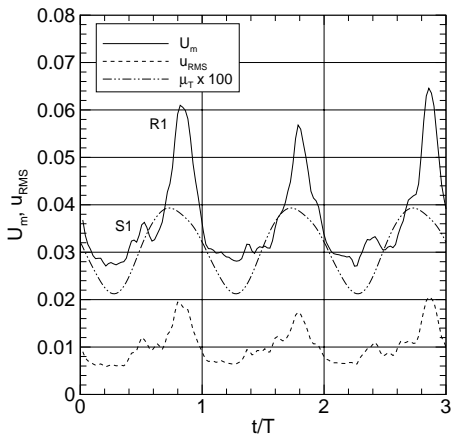


Figure 20. HOT FILM PROBE, inlet stator 2, computed viscosity μ_T against measured phase averaged anemometer output voltage U_m and random unsteadiness U_{rms} .

Figure 23 shows the space time diagram of the wall shear stress on the suction side of the stator blade two for the unsteady computation with transition for three blade passing periods for a distinct stator one position (position a) for the first clocking pair. The wake passing of the rotor wake, indicated by the trajectories

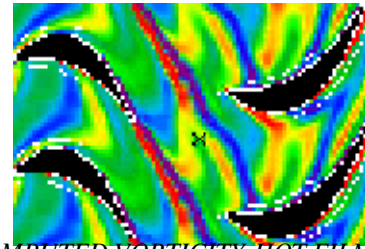


Figure 21. COMPUTED VORTICITY, HOT FILM PROBE INDICATED WITH A CROSS.

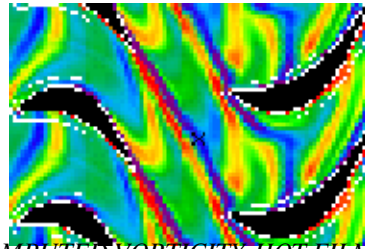


Figure 22. COMPUTED VORTICITY, HOT FILM PROBE INDICATED WITH A CROSS.

of the leading edge and the trailing edge of the rotor wake (R1), yields a higher skin friction at the wall for the meridional coordinate MMG at values of about 0.5 and the dimensionless time of about 0.8 for the numerical results as well as the experiments. The influence of the wake gives also higher wall shear stress levels at the trailing edge (MMG=0.95, $t/T=1.5$), which is in agreement with the experimental data in figure 24 given as quasi wall shear stress. Moreover, the stator one wake (S1) leads to another local maximum at MMG = 0.75 and a dimensionless time of 0.5, which cannot be detected in the experiments. The global minimum found in the experiments at MMG=0.85 and $t/T=0.9$ is also predicted in the numerical results but slightly downstream at MMG=0.95. The so-called equalizing effect mentioned in part one of this paper due to the stator wake is visible in the numerical as well as the experimental results. It leads to a smaller local increase of wall shear stress in the wake induced path of the rotor wake for the numerical results as well as the measurements at the trailing edge.

Figure 25 shows the space time diagram of the wall shear stress on the suction side of the stator two for the computation with transition for three blade passing periods for another distinct stator one position (position b) of the first clocking pair. The numerical results given in figure 25 and the experimental results in figure 26 show clearly the wake induced path (R1) which leads to higher (quasi) wall shear stress level. The computations do not show a second local minimum as observed for the stator one position a in agreement with the experiments, which does not show the so-called equalizing effect described in part one of this paper. The global minimum found in the experiments at MMG=0.85 and $t/T=0.8$ is predicted in the numerical results as well, however at a slightly different position.

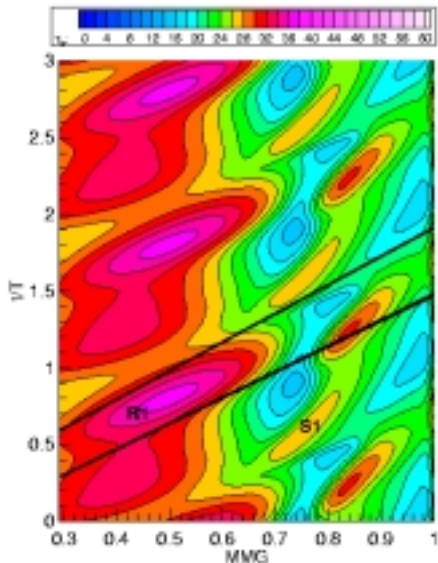


Figure 23. WALL SHEAR STRESS, SUCTION SIDE STATOR 2, transition model on, position a for stator one.

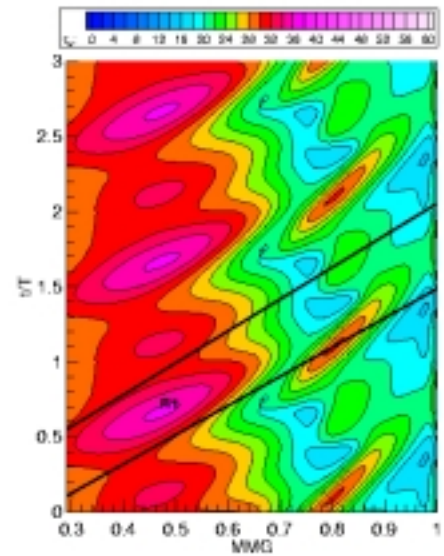


Figure 25. WALL SHEAR STRESS, SUCTION SIDE STATOR 2, transition model on, position b for stator one.

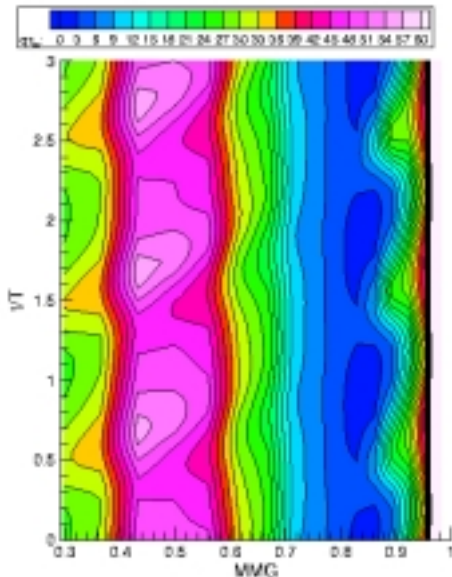


Figure 24. QUASI WALL SHEAR STRESS, SUCTION SIDE STATOR 2, experiments, position a for stator one.

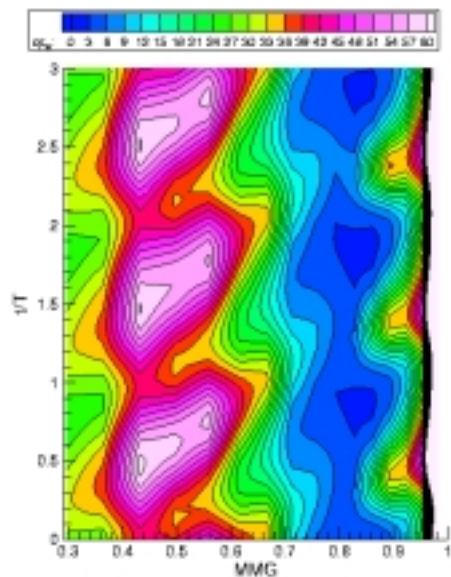


Figure 26. QUASI WALL SHEAR STRESS, SUCTION SIDE STATOR 2, experiments, position b for stator one.

CONCLUSIONS

A time-accurate Navier-Stokes solver is applied towards the unsteady flow interaction in three stage low pressure turbine. A modern one equation turbulence model coupled with a variant of an AGS transition model is used to predict the transition on the blade surface.

The steady and unsteady time averaged results show good agreement with the experiments for the surface pressure distribution at midspan.

The unsteady interaction of the wake of an upstream stator with

the following rotor and the next stator is correctly predicted as a comparison of the contour plot and available hot film probe data shows.

Reasonable qualitative agreement between numerical results and experimental data is found for the wall shear stress for two distinct stator one positions. Future investigations will show if a better agreement can be achieved.

The present results show that the wake of the stator one has a strong impact on the hot film probe measurements in front of stator two as well as on the hot film data on the suction side of

stator two and only a weak influence on the unsteady pressure distribution.

ACKNOWLEDGMENT

The authors would like to thank MTU for permission to publish the results. Moreover, the authors would like to thank Dr. A. Fiala for the many useful discussions about the analysis of the experimental data. The work is part of the "Engine 3E 2010 Programm" financed by the German Ministry of Economics and Technology under the contract number 20T9605. The financial support is gratefully acknowledged.

REFERENCES

- Abu-Ghannam, B. and Shaw, R., 1980, "Natural Transition of Boundary Layers The Effects of Turbulence, Pressure Gradient and Flow History.", J. of Mech. Engineering Science, Vol. 22, pp. 213 - 228.
- Boussinesq, T. V., 1877, *Mem. pres Acad. Sci.*, 3rd edn. Paris XXIII, p. 46.
- Coupland, J., 1995, "Transition Modelling for Turbomachinery Flows.", ERCOFTAC bulletin, Vol. 24, pp. 5 - 8.
- Dorney D.J., Sondak D.L., Cizmas, P.G.A., Saren, V.E., Savin, N.M., 1999, "Full-Annulus Simulations of Airfoil Clocking in a 1 1/2 Stage Axial Compressor.", ASME, 98-GT-23.
- Dorney D.J. and Sondak D.L., 2000, "Three-Dimensional Simulations of Airfoil Clocking in a 1 1/2 Stage Turbine.", AIAA 2000-3359.
- Drela, M., 1995, "MISES Implementation of Modified Abu-Ghanam/Shaw Transition Criterion.", MIT Aero-Astro, February 1995.
- Ekaterinaris, J.A., 1995, *Numerical Investigation of Dynamic Stall of an Oscillating Wing*., AIAA Journal, Vol. 33, No. 10, pp. 1803 - 1808.
- Engel, K., Eulitz, F., Pokorny, S. and Faden, M., 1996 *Validation of Different TVD-Schemes for the Calculation of the Unsteady Turbomachinery Flow*., 14. ICNMF, Bangalore, India.
- Eulitz F. and Engel K., 1998, "Numerical Investigation of Wake Interaction in a Low Pressure Turbine.", ASME, 98-GT-563, Stockholm.
- Eulitz, F., Engel, K., Nürnberger, D., Schmidt, S. and Yamamoto, K., 1998, "On Recent Advances of a Massively-Parallel Time-Accurate Navier-Stokes Solver for Unsteady Turbomachinery Flow.", Proceedings ECCOMAS, Athens.
- Fan, S. and Lakshminarayana, B., 1996, "Computation and Simulation of Wake-Generated Unsteady Pressure and Boundary Layers in Cascades, Part 1 - 2.", ASME J. of Turbomachinery, Vol. 118, pp. 96 - 121.
- Giles, M., 1991, "UNSFLO: A Numerical Method for the Calculation of Unsteady Flow in Turbomachinery.", GTL-Report 205, MIT-GTL.
- Halstead, D.E., Wisler, D.C. Okiishi, T.H., Walker, G.J., Hodson, H.P. and Shin, H.-W., 1997 "Boundary Layer Development in Axial Compressors and Turbines: Part 1 -4.", ASME Journal of Turbomachinery, Vol. 119, pp. 114-139; 225-237; 426-444.
- He, L., 1993, "New Two-Grid Acceleration Method for Unsteady Navier-Stokes Calculations.", J. Prop. and Power, Vol. 9, p.272.
- Hodson, H.P., Huntsmann, L. and Steele, A.B., 1994, "An Investigation of Boundary Layer Development in a Multistage LP Turbine.", Journal of Turbomachinery, Vol. 116, pp. 375-383.
- Hodson, H.P., 1998, "Blade Row Interference Effects in Axial Turbomachinery Stages: Blade Row Interactions in Low Pressure Turbines.", VKI Lecture, Brussels, February 1998.
- Hoying, D. A., 1997, "Approximate Unsteady Non-Reflecting Boundary Conditions for the Three-Dimensional Euler Equations.", AIAA Paper 97-2739.
- Huber F.W., Johnson P.D., Sharma O.P., Staubach J.B., Gaddis S.W., 1995, "Performance Improvement Through Indexing of Turbine Airfoils: Part 1-Experimental Investigation.", ASME Journal of Turbomachinery, Vol. 118, pp. 630-635.
- Narasimha, R., 1990, "Modelling the Transitional Boundary Layer.", NASA CR-187487, ICASE Report No. 90-90.
- Niehuis R.; 1997, "Luftfahrtforschung und -technologie Engine 3E 2010 Programm für zivile MTU- Antriebsprojekte, Turbinen für Triebwerke der unteren Schubklasse Phase A.", Daimler-Benz Aerospace MTU München.
- Roe, P., 1981, "Approximative Riemann Solvers, Parameter Vector and Differences Schemes.", J. Comp. Physics, Vol. 43, pp. 357 - 372.
- Savill, A.M., 1994, "Transition Modelling for Turbomachinery.", Proc. ERCOFTAC Turbomachinery Special Interest Group Seminar and Workshop on 3D Turbomachinery Flow Prediction, Part 2.
- Saxer, A.P. and Giles, M., 1993, "Quasi Three Dimensional Nonreflecting Boundary Conditions for Euler Equations Calculations.", AIAA J. Propulsion and Power, Vol. 9, No. 2, pp. 263 - 271.
- Sharma, O., 1998, "Blade Row Interference Effects in Axial Turbomachinery Stages.", VKI Lecture, Brussels, February 1998.
- Solomon, W.J., 2000, "Effects of Turbulence and Solidity on the Boundary Layer Development in a Low Pressure Turbine.", ASME, 2000-GT-0273, Munich.
- Spalart, P. and Allmaras, S., 1992, "A One-Equation Turbulence Model for Aerodynamic Flows.", AIAA 92-0439.
- van Leer, B., 1979, "Towards the Ultimate Conservation Difference Scheme, A Second Order Sequel to Godunov's Method.", J. Comp. Physics, Vol. 32, pp. 101 - 136.